

## INVESTIGATION OF STRUCTURE AND PROPERTIES OF MELT-SPUN NiTi BASED SHAPE MEMORY ALLOYS

Kieu Xuan Hau<sup>1,2,\*</sup>, Nguyen Hai Yen<sup>1,2</sup>, Nguyen Huy Ngoc<sup>1,2</sup>, Truong Viet Anh<sup>2</sup>,  
Pham Thi Thanh<sup>1,2</sup>, Nguyen Van Toan<sup>1,2</sup>, Tran Dang Thanh<sup>1,2</sup>, Nguyen Huy Dan<sup>1,2</sup>

<sup>1</sup>*Institute of Materials Science, Vietnam Academy of Science and Technology,  
18 Hoang Quoc Viet, Cau Giay, Ha Noi, Viet Nam*

<sup>2</sup>*Graduate University of Science and Technology, Vietnam Academy of Science and Technology,  
18 Hoang Quoc Viet, Cau Giay, Ha Noi, Viet Nam*

\*Email: haukx@ims.vast.ac.vn

Received: 15 August 2021; Accepted for publication: 20 June 2022

**Abstract.** In this work, we investigated the structure, mechanical properties and corrosion resistance of Ti<sub>50</sub>Ni<sub>50</sub> and Ti<sub>16.667</sub>Zr<sub>16.667</sub>A<sub>16.667</sub>Ni<sub>25</sub>Cu<sub>25</sub> (A = Hf, Nb, Co, Cr and Ga) shape memory alloys (SMAs) fabricated by using melt-spinning method. X-ray diffraction (XRD) and scanning electron microscopy (SEM) analyses reveal that the alloy ribbons are partially crystallized with B19' martensitic structure in the added alloys. The crystalline phase formation and the atomic size difference ( $\delta = 4.33 - 10.25\%$ ) significantly affect the hardness, tensile strength, tensile strain, elastic modulus and corrosion resistance of the alloys. The hardness of the alloy gradually increases from 583 HV to 873 HV when adding elements in the order of Hf, Nb, Co, Cr and Ga. Tensile strength, tensile strain and elastic modulus simultaneously reach their maximum of 669.2 MPa, 0.899% and 28.82 GPa, respectively, when Hf is added to the alloy. Ga enhances the corrosion resistance of the alloy ribbons more than other additional elements.

**Keywords:** Shape memory effect, shape memory alloy, structural transformation, martensitic-austenitic transformation, melt-spinning method.

**Classification numbers:** 2.2.1.

### 1. INTRODUCTION

NiTi based shape memory alloys (SMAs) are renowned not only for good shape memory characteristics, mechanical properties and corrosion resistance but also for high biocompatibility [1 - 3]. However, the applications of the NiTi alloys at high temperatures are limited due to their low transformation temperatures (below 100 °C) [4, 5]. To have the great potential for the application of SMAs at high temperatures, researchers have been attempting to increase the transformation temperatures of SMAs by adding elements such as Hf, Zr, Cu and Nb into the NiTi based alloys [5 - 7]. Recently, some scientists have discovered the shape memory effect (SME) on high-entropy alloys (HEAs). The HEA was defined by Yeh et al. [8] that it contains at least five metallic elements, and each element has a concentration of 5 - 35 atomic percent. High-entropy shape memory alloys (HESMAs) were first proposed by Firstov et

al. [9]. They combined a high-temperature shape memory alloy (HTSMA) with an HEA and successfully developed the CoCuNiHfTiZr HESMA, in which Ti was partially replaced by Zr and Hf, and Ni was partially substituted by Co and Cu. The authors demonstrated that the  $\text{Ti}_{16.667}\text{Zr}_{16.667}\text{Hf}_{16.667}\text{Ni}_{25}\text{Cu}_{25}$  alloy can undergo a martensitic transformation with the starting temperature  $M_s$  of 226 °C and an austenitic transformation with the finishing temperature  $A_f$  of 338 °C [10]. They proposed that HESMAs have a potential to be applied as HTSMAs [11]. Other authors have indicated that the  $\text{Ti}_{16.67}\text{Zr}_{16.67}\text{Hf}_{16.67}\text{Ni}_{25}\text{Co}_{10}\text{Cu}_{15}$  HESMA undergoes a transformation from high temperature austenitic phase (B2) to low temperature martensitic phase (B19'). Besides, this HESMA shows recoverable strain and tensile strength of 4.8 % and 650 MPa, which are comparable to those of the NiTi alloy of 4.9 % and 200 MPa, respectively [12, 13]. In a recent study, Canadinc et al. have found HESMAs of  $(\text{Ni}, \text{Pd})_{50}(\text{Ti}, \text{Hf}, \text{Zr})_{50}$  with the  $A_f$  above 700 °C [14]. They showed that HESMAs can significantly improve the transformation temperatures and recovery strain. In this work, we investigated the structure and properties of NiTi based HESMAs fabricated by using melt-spinning method.

## 2. EXPERIMENTAL

Pre-alloys with nominal compositions of  $\text{Ti}_{50}\text{Ni}_{50}$  and  $\text{Ti}_{16.667}\text{Zr}_{16.667}\text{A}_{16.667}\text{Ni}_{25}\text{Cu}_{25}$  (A = Hf, Nb, Co, Cr and Ga) were prepared from pure metals (99.9 %) of Ti, Ni, Cu, Zr, Hf, Nb, Co, Cr and Ga. After being chopped and cleaned, the raw materials were weighed according to the molar percentages of the elements. Then, the samples were melted by an arc furnace under Ar gas. The sample chamber was evacuated to about 1.5 Pa. The chamber was charged and discharged with Ar gas several times to remove impurities. Then, the sample chamber was filled with Ar gas to a pressure of about  $12.10^4$  Pa. A getter of Ti was arc-melted several times to get contaminant gases before melting the samples. Each sample was melted and turned over 5 times to ensure its homogeneity. After arc-melting, the pre-alloys were used to fabricate ribbons on a melt-spinning system with the same tangential velocity,  $v = 40$  m/s, of the copper roller. The fabricated ribbons are about 2 mm wide and 30  $\mu\text{m}$  thick. The ribbon samples are symbolized and listed in Table 1.

Table 1. Symbols and percentage of the molar concentration of the elements in the alloy ribbons (with A = Hf, Nb, Co, Cr and Ga).

Symbols	Ni (%mol)	Ti (%mol)	Zr (%mol)	Cu (%mol)	A (%mol)
S1	50	50	0	0	0
S2	25	50/3	50/3	25	50/3 (Hf)
S3	25	50/3	50/3	25	50/3 (Nb)
S4	25	50/3	50/3	25	50/3(Co)
S5	25	50/3	50/3	25	50/3(Cr)
S6	25	50/3	50/3	25	50/3 (Ga)

The microstructure and grain size of the alloy ribbons were investigated by using XRD and SEM methods. The mechanical properties of the ribbons were studied by using the stress-strain

and micro-hardness measurements according to ISO-178 and ISO-76520 standards. The corrosion resistance of the ribbons was investigated by measuring the anodic polarization curve. The electrochemical experiments were conducted in a standard three-electrode cell corrosion tester (PCPA *i*oc HH5) which included a working electrode, a platinum mesh as a counter electrode and a reference electrode of Ag. The electrochemical corrosion tests were carried out in 3.5 % NaCl solution with a pH of 7.14 at a temperature of  $36.5 \pm 1$  °C.

### 3. RESULTS AND DISCUSSION

According to the results of our previous study [15], the S1, S2, S3, S4 and S5 alloy ribbons are single phases of B19' (martensite) or multi-phases of B19' and B2 (austenite) at room temperature. The S1 sample exhibits complete crystallization, while the others reveal partial crystallization.

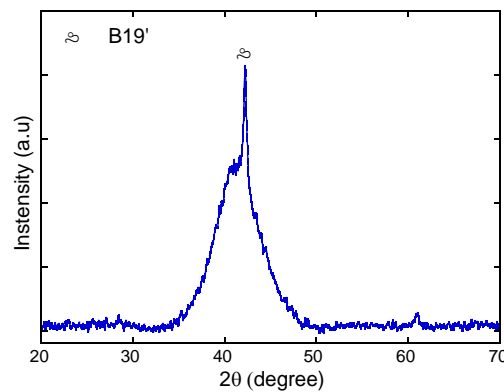


Figure 1. XRD pattern of the S6 alloy ribbon.

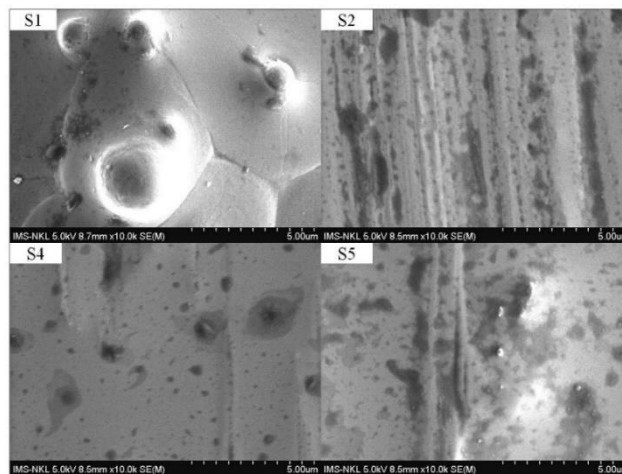


Figure 2. SEM image of the surface of free-side of the S1, S2, S4 and S5 alloy ribbons.

Figure 1 presents the result of XRD pattern of the S6 alloy ribbons. Accordingly, the S6 alloy ribbons only have a diffraction peak of B19' phase appeared on its XRD pattern, similar to those of the HESMAs studied in our previous work [15]. The structural transformation of the NiTi based SMAs from B19' to B2 was observed by using XRD measurements at high

temperature and differential scanning calorimetry (DSC) analyses [15]. By addition of Zr, Cu, Cr, Co, Nb and Hf, the structural transformation from B19' to B2 in the NiTi based alloys occurs at higher temperatures in the range of 500 - 650 °C [15].

Figure 2 presents the microstructure of the S1 and the S2, S4 and S5 HESMAs. The SEM results are completely consistent with those of the XRD analysis in the previous study [15]. For the S1 alloy ribbon, we can clearly observe the grain boundary and the grain size of 3 - 4 μm. It is clear that this sample is completely crystallized. For the HESMA samples, the crystallization process is partial. Therefore, their grain boundaries are not observed. The influence of microstructure on the properties of the alloy ribbons is shown in the following section.

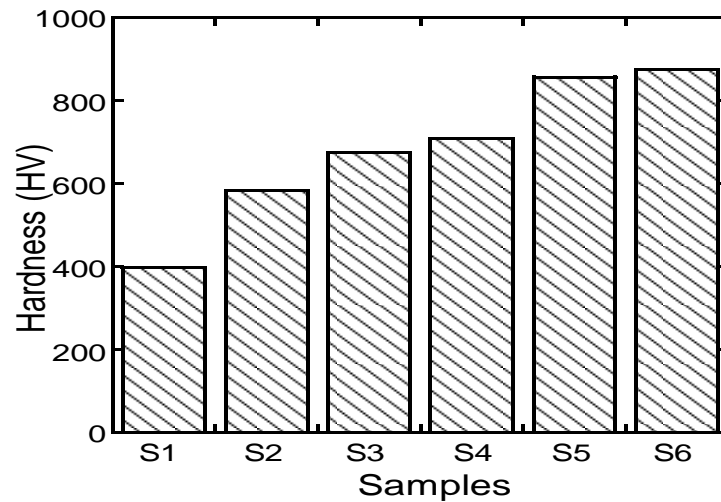


Figure 3. Vickers Hardness (HV) of the alloy ribbons.

Figure 3 shows the results of hardness measurements of the alloy ribbons (specific values are listed in Table 2). The S1 sample has a hardness of 398 HV. After adding elements to the alloy, we found that the hardness of the alloy ribbons significantly increases above 500 HV. The S2 sample has the lowest hardness of 583 HV, while the S6 sample has the highest hardness of 873 HV. The substitution of Cu, Zr, Co, Nb, Hf, Cr and Ga elements for Ti and Ni at the initial lattice nodes leads to lattice distortion. That means the formation of lattice distortion leads to improve mechanical properties of the samples. The lattice distortion is formed due to the atomic size difference ( $\delta\%$ ) of the alloy ribbons. The value  $\delta$  is determined by Equation 1 [16]:

$$\delta = \sqrt{\sum_{i=1}^n c_i \left(1 - \frac{r_i}{\bar{r}}\right)^2} \quad (1)$$

where  $n$  is the number of the components in an alloy system,  $c_i$  is the atomic percent of the  $i$  element,  $r_i$  is the atomic radius of the  $i$  component [17],  $\bar{r}$  is the average atomic radius with

$$\bar{r} = \sum_{i=1}^n c_i \cdot r_i$$

The  $\delta$  parameters are calculated from Equation 1 of the S1, S2, S3, S4, S5, and S6 samples corresponding to 4.33, 10.25, 9.08, 9.62, 9.66 and 9.88 %, respectively. The results reveal that the hardness of the HEAs tends to increase when the  $\delta$  increases. It also proves that the lattice deformation leads to an improvement in the mechanical properties of the alloy ribbons. Table 2 shows a comparison of the Vickers hardness of the alloys studied in this work with those of the

HEAs reported previously.

*Table 2.* Comparison of the Vickers hardness of the alloys studied in this work with those of the HEAs reported previously.

Nominal composition	Hardness (HV)	Reference
S1	398	This work
S2	583	This work
S3	674	This work
S4	708	This work
S5	856	This work
S6	873	This work
Ti <sub>40</sub> Zr <sub>10</sub> Ni <sub>40</sub> Co <sub>5</sub> Cu <sub>5</sub>	409	[18]
Ti <sub>30</sub> Zr <sub>20</sub> Ni <sub>30</sub> Co <sub>10</sub> Cu <sub>10</sub>	517	[18]
Ti <sub>25</sub> Zr <sub>25</sub> Ni <sub>16.67</sub> Co <sub>16.67</sub> Cu <sub>16.67</sub>	538	[18]
Ti <sub>20</sub> Zr <sub>15</sub> Hf <sub>15</sub> Ni <sub>20</sub> Co <sub>15</sub> Cu <sub>15</sub>	572	[18]
Ti <sub>30</sub> Zr <sub>10</sub> Hf <sub>10</sub> Ni <sub>30</sub> Co <sub>10</sub> Cu <sub>10</sub>	526	[18]
TiZrHfNbTa	383	[19]
TiZrNbVCr	481	[20]

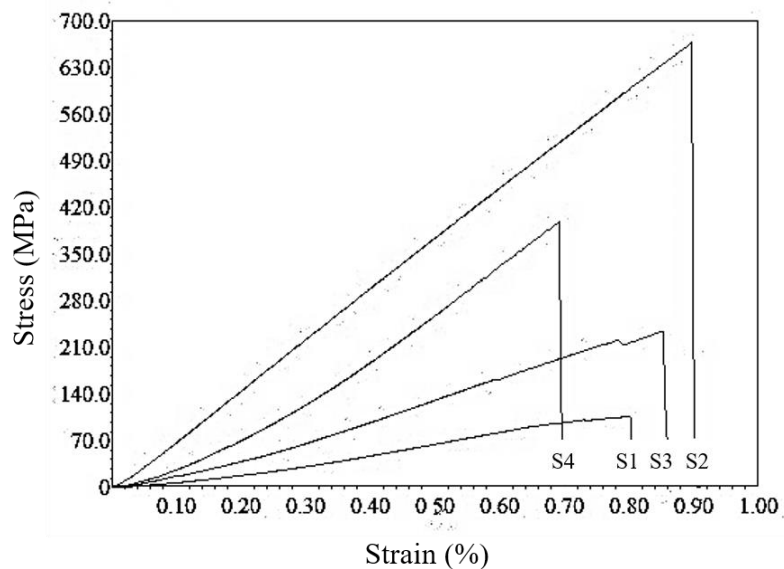


*Figure 4.* Stress-strain curves of alloy ribbons.

The stress-strain curves of the alloy ribbons are shown in Figure 4. One can see that the stress-strain curves have two distinct zones. The first zone is the linear elastic region and the

other is the destruction region. The linear elastic region is the area of material that is able to recover after unloading. It means that the material has the ability to return to its original shape completely or partially after unloading. The destruction region is the maximum load that the material can withstand before forming microcracks leading to the destruction. It can be seen that the stress-strain curves of the alloy ribbons do not appear in the plastic deformation region. The values of tensile strength, tensile strain and elastic modulus are listed in Table 3. It can be seen that the S2, S3, and S4 HESMAs have higher tensile strength and elastic modulus than those of the S1 sample. The tensile strength and elastic modulus increase with the increasing atomic size difference. The atomic size difference of the S1, S2, S3 and S4 alloy ribbons is sorted in the following order  $S1 < S3 < S4 < S2$ . Therefore, the tensile strength and elastic modulus values of the S1, S2, S3 and S4 alloy ribbons also follow the above order. However, the tensile strain of the samples increases slightly. The atomic radius size difference of the alloy ribbons improves the mechanical properties. Specifically, the HESMAs have a higher  $\delta$  than that of the S1 sample.

Table 3. Tensile strength, tensile strain and elastic modulus values of alloy ribbons.

Samples	Tensile strength (MPa)	Tensile strain (%)	Elastic Modulus (GPa)
S1	106.3	0.8	5.64
S2	669.2	0.899	28.82
S3	234.9	0.854	24.19
S4	399.5	0.692	27.54

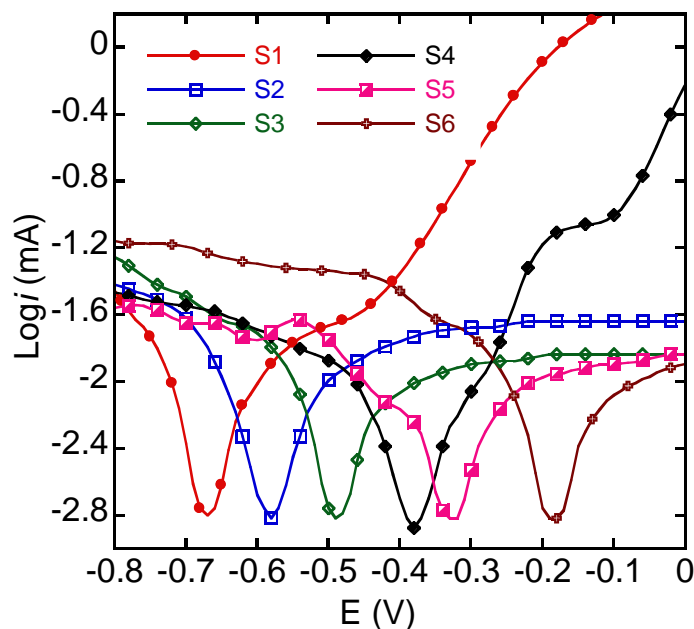


Figure 5. The anodic polarization curves of the alloy samples in 3.5 % NaCl solution.

Figure 5 shows the anodic polarization curves for the SMAs measured in 3.5 wt.% NaCl solution and a reference electrode of Ag. The corrosion potential ( $E_{\text{corr}}$ ) and corrosion current density ( $i_{\text{corr}}$ ) calculated by the Tafel extrapolation method are given in Table 4. It can be seen that the corrosion potential of the samples tends to increase from -670 mV to -190 mV corresponding to the S1, S2, S3, S4, S5 and S6 samples, respectively, while their corrosion current density decreases from  $2.63 \times 10^{-5}$  to  $0.86 \times 10^{-5}$  A/cm<sup>2</sup>. This means that the electrochemical corrosion resistance of the HESMAs in the 3.5 % NaCl solution significantly increases compared to the NiTi SMA (S1). For the S2, S3, S4, S5 and S6 HESMAs, the corrosion potential strongly increases from -580 mV to -190 mV. However, the corrosion current density does not follow any rule. The maximum and minimum  $I_{\text{corr}}$  values are  $2.63 \times 10^{-5}$  A/cm<sup>2</sup> for the S5 sample and  $0.86 \times 10^{-5}$  A/cm<sup>2</sup> for the S6 sample, respectively. The presence of Ga in the S6 alloy ribbons increases the corrosion resistance but decrease the corrosion current density several times compared with the Hf, Nb, Co, and Cr-containing alloy ribbons.

Table 4.  $E_{\text{corr}}$  and  $i_{\text{corr}}$  of samples tested in 3.5 % NaCl aqueous solutions.

Samples	$i_{\text{corr}}$ (A/cm <sup>2</sup> )	$E_{\text{corr}}$ (mV)
S1	$2.62 \times 10^{-5}$	-670
S2	$2.03 \times 10^{-5}$	-580
S3	$2.35 \times 10^{-5}$	-480
S4	$2.1 \times 10^{-5}$	-370
S5	$2.63 \times 10^{-5}$	-330
S6	$0.86 \times 10^{-5}$	-190

#### 4. CONCLUSIONS

The SMA of Ti<sub>50</sub>Ni<sub>50</sub> and HESMAs of Ti<sub>16.667</sub>Zr<sub>16.667</sub>A<sub>16.667</sub>Ni<sub>25</sub>Cu<sub>25</sub> (A = Hf, Nb, Co, Cr and Ga) have been studied for microstructure, hardness, tensile strain, tensile strength, modulus elastic and corrosion resistance. The phase formation and the atomic size difference of the alloy ribbons significantly affect their structure, mechanical and corrosion properties. All the mechanical properties and corrosion resistance of the alloy are enhanced by the addition of the investigated elements. The hardness of the alloy gradually increases from 583 HV to 873 HV when adding elements in the order of Hf, Nb, Co, Cr and Ga. Tensile strength, tensile strain and elastic modulus simultaneously reach their maximum of 669.2 MPa, 0.899 % and 28.82 GPa, respectively, when Hf is added to the alloy. The Ga-containing ribbon has the best electrochemical corrosion resistance with the corrosion potential and current density values of -190 mV and  $0.86 \times 10^{-5}$  A/cm<sup>2</sup>, respectively.

**Acknowledgements.** This work was supported by the National Foundation for Science and Technology Development (NAFOSTED) of Viet Nam under grant number 103.02-2019.344. A part of the work was done in the Key Laboratory for Electronic Materials and Devices, IMS-VAST.

**CRedit authorship contribution statement.** Kieu Xuan Hau: Curation data, Writing original draft. Nguyen Huy Ngoc, Truong Viet Anh: Fabrication samples. Pham Thi Thanh, Tran Dang Thanh: Measurement. Nguyen Hai Yen, Nguyen Van Toan: Analysis data. Nguyen Huy Dan: Supervision, Revising manuscript.

**Declaration of competing interest.** The authors declare that they have no known competing financial interests or personal relationships that could have appeared to influence the work reported in this paper.

## REFERENCES

1. Otsuka K., Ren X. - Physical metallurgy of Ti-Ni-based shape memory alloys, *Prog.Mater. Sci.* **50** (2005) 511-679. <https://doi.org/10.1016/j.pmatsci.2004.10.001>.
2. Jani J., Leary M., Subic A., Gibson M. - A review of shape memory alloy research, applications and opportunities, *Materials & Design.* **56** (2014) 1078-1113. <https://doi.org/10.1016/J.MATDES.2013.11.084>.
3. Figueira N., Silva M., Carmezim J., Fernandes S. C. - Corrosion behaviour of NiTi alloy, *Electrochim Acta.* **54** (2009) 921-926. <https://doi.org/10.1016/j.electacta.2008.08.001>.
4. Ma J., Karaman. I, Noebe. D. R. - High temperature shape memory alloys, *Int.Mater.Rev.* **55** (2010) 257-315. <https://doi.org/10.1179/095066010X12646898728363>
5. Thoma P., Boehm J. - Effect of composition on the amount of second phase and transformation temperatures of Ni<sub>x</sub>Ti<sub>90-x</sub>Hf<sub>10</sub> shape memory alloys, *Mat. Sci. Eng. A* **273** (1999) 385-389. [https://doi.org/10.1016/S0921-5093\(99\)00303-2](https://doi.org/10.1016/S0921-5093(99)00303-2).
6. Fu B., Feng K., Zhuguo L. - Study on the effect of Cu addition on the microstructure and properties of NiTi alloy fabricated by laser cladding, *Mater. Lett.* **220** (2018) 148-151. <https://doi.org/10.1016/j.matlet.2018.03.030>.
7. Humbeeck V. J. - High temperature shape memory alloys, *J. Eng. Mater. Technol* **121** (1999) 98-101. <https://doi.org/10.1177/1045389X06063922>.
8. Yeh J., Chen S., Lin S., Gan J., Chin T., Shun T., Tsau C. - Nanostructured High-Entropy Alloys with Multiple Principal Elements: Novel Alloy Design Concepts and Outcomes, *Adv. Eng. Mater.* **6** (2004) 299-303. <http://doi.wiley.com/10.1002/adem.200300567>.
9. Firstov G., Timoshevski A., Kosorukova T., Koval Y., Matviychuk Y., Verhovlyuk P. - Electronic and crystal structure of the high entropy TiZrHfCoNiCu intermetallics undergoing martensitic transformation, *Matec. Web. Confer.* **33** (2015) 06006. <http://doi:10.1051/mateconf/20153306006>
10. Firstov G., Kosorukova T., Koval Y., Odnosum V. - High entropy shape memory alloys, *Proceedings of International Conference on Martensitic Transformations ICOMAT-2014, Vol. 2, 2015 pp.* 499-504.
11. Firstov G., Kosorukova T., Koval Y., Verhovlyuk P. - Directions for High-Temperature Shape Memory Alloys' Improvement: Straight Way to High-Entropy Materials, *Shap. Mem. Superelasticity.* **1** (2015) 400-407. <http://doi:10.1007/s40830-015-0039-7>.
12. Chen H. C., Chen J. Y. - Shape memory characteristics of (TiZrHf)<sub>50</sub>Ni<sub>25</sub>Co<sub>10</sub>Cu<sub>15</sub> high entropy shape memory alloy, *Scrip. Mater.* **162** (2019) 185-189. <http://doi:10.1016/j.scriptamat.2018.11.023>
13. Chen H. C., Chen J. Y., Shen J. J. - Microstructure and Mechanical Properties of (TiZrHf)<sub>50</sub>(NiCoCu)<sub>50</sub> High Entropy Alloys, *Met. Mater. Inter.* **26** (2020) 617-629. <http://doi:10.1007/s12540-019-00383-3>.
14. Canadinc D., Trehern W., Ma J., Karaman I., Sun F., Chaudhry Z. - Ultra-high temperature multi-component shape memory alloys, *Scrip. Mater.* **158** (2019) 83-87 (2019).<http://doi:10.1016/j.scriptamat.2018.08.019>.

15. Dan H. N., Thanh D. T., Thanh T. P., Ngoc H. N., Nuoi D. D., Yen H. Y., Dai V. P. - Investigation of Shape Memory Effect in Ni-Ti Based Alloys, Proceedings of The 10<sup>th</sup> National Conference of Solid State Physics and Materials Science, Quy Nhon University, 2019, pp. 152-155.
16. Zhang Y., Zhou Y., Lin J., Chen G., Liaw P. - Solid-solution phase formation rules for multi-component alloys, *Adv. Eng. Mat.* **10** (2008) 534-538. <http://doi:10.1002/adem.200700240>.
17. James S. G. - Lange's Handbook of Chemistry, McGraw-Hill, New York, 2004.
18. Chen H. C, Chen J. Y., Shen J. Y. - Microstructure and Mechanical Properties of (TiZrHf)<sub>50</sub>(NiCoCu)<sub>50</sub> High Entropy Alloys, *Met. Mater. Inter.* **26** (2020) 617-629. <https://doi.org/10.3390/e21101027>
19. Senkov O. N., Scott J. M., Senkova S. V., Miracle D. B., Woodward C. F. - Microstructure and room temperature properties of a high-entropy TaNbHfZrTi alloy, *J. Alloys. Compd.* **509** (2011) 6043-6048. <https://doi.org/10.1016/j.jallcom.2011.02.171>.
20. Senkov O., Senkova S., Miracle D., Woodward C. - Mechanical properties of low-density, refractory multi-principal element alloys of the Cr-Nb-Ti-V-Zr system, *Mater. Scie. Eng A*, **565** (2013) 51-62. <http://doi:10.1016/j.msea.2012.12.018>